# Production of neutron-rich $^{209–212}$Pt isotopes based on a dinuclear system model

Gen Zhang,[1,2] Cheng Li,[2] Pei-Wei Wen,[3] Jing-Jing Li,[1,2] Xin-Xin Xu,[1,2] Bing Li,[1,2] Zhong Liu,[4] and Feng-Shou Zhang[1,2,5,*]

[1]*The Key Laboratory of Beam Technology and Material Modification of Ministry of Education, College of Nuclear Science and Technology, Beijing Normal University, Beijing 100875, China*

[2]*Beijing Radiation Center, Beijing 100875, China*

[3]*China Institute of Atomic Energy, Beijing 102413, China*

[4]*Institute of Modern Physics, Chinese Academy of Sciences, Lanzhou 730000, China*

[5]*Center of Theoretical Nuclear Physics, National Laboratory of Heavy Ion Accelerator of Lanzhou, Lanzhou 730000, China*

(Received 8 May 2018; published 23 July 2018)

The production cross sections of new neutron-rich nuclei $^{209–212}$Pt are investigated with multinucleon transfer reactions by the dinuclear system model. It is found that the $^{133}$Sn + $^{204}$Hg and $^{145}$Xe + $^{208}$Pb systems are advantageous to produce the neutron-rich nuclei, in which the production cross sections are much higher than those produced in projectile fragmentation reactions. The optimal incident energies for these two systems are about 1.18 and 1.40 times the Coulomb barrier, respectively. The highest cross sections of unknown isotopes $^{209–212}$Pt in the $^{145}$Xe + $^{208}$Pb reaction are 2.7 nb, 0.4 nb, 8.2 pb, and 2.7 pb, respectively, and those for the $^{133}$Sn + $^{204}$Hg reaction are 1.7 nb, 0.4 nb, 23.3 pb, and 4.8 pb, respectively.

DOI: 10.1103/PhysRevC.98.014613

## I. INTRODUCTION

The synthesis of new neutron-rich nuclei located around the neutron closed shell $N = 126$ is highly interesting in nuclear physics. On the one hand, it is very important to extend our knowledge of the structure and decay properties of extremely neutron-rich nuclei. On the other hand, the neutron magic number $N = 126$ is the last waiting point on the path of the $r$ process [1,2]. To produce nuclei around the $N = 126$ shell is significant for understanding the $r$ process of astrophysical nucleosynthesis. Many new isotopes around the $N = 126$ shell have been produced by means of projectile fragmentation reactions of $^{238}$U in recent years [3–6]. However, this region still remains a large blank area in the nuclear chart. For example, there have been only 11 neutron-rich Pt isotopes produced successfully up to now.

The production methods of the known neutron-rich Pt isotopes are summarized in Table I. The abbreviations LP, NC, and PF in the Table I represent light-particle-induced reaction, neutron capture reaction, and projectile fragmentation reaction, respectively. $^{197,199–202}$Pt were observed by NC or LP reactions [7–11]. More neutron-rich Pt isotopes, produced in PF reactions, have extremely low yields [4,6,12]. For example, in the reaction of 1 GeV/nucleon $^{238}$U with $^{9}$Be performed at Gesellschaft für Schwerionenforschung (GSI), the cross sections of $^{206–208}$Pt are 2.7 pb, 8 pb, and 3.3 pb, respectively [6]. Limited by current detection techniques, it is not easy to obtain Pt isotopes with mass numbers above 208 through the PF method.

Since the multinucleon transfer (MNT) reaction was proposed to produce new neutron-rich heavy and superheavy nuclei by Zagrebaev *et al.*, the MNT reaction has attracted renewed interest in recent years [13–19]. Both experimental [20–26] and theoretical [14,27–30] results demonstrate that the MNT reaction in low-energy heavy-ion collisions may be a promising path to produce exotic neutron-rich nuclei around $N = 126$. Especially for the $^{136}$Xe + $^{198}$Pt reaction at 7.98 MeV/nucleon performed at GANIL, the experimental result shows that the production cross sections of nuclei along the $N = 126$ shell are significantly greater than those produced in the PF method [22]. The transfer reaction $^{136}$Xe + $^{208}$Pb at $E_{\mathrm{c.m.}} = 450$ MeV performed at Argonne National Laboratory (ANL) yielded the most neutron-rich Pt isotope reached, $^{202}$Pt, at the level of 0.1 mb [23].

Some semiclassical and microscopic models have been developed to describe the MNT processes in heavy-ion collisions. The dinuclear system (DNS) model [31–33], the grazing model [34,35], Langevin equations [36,37], and the complex Wentzel-Kramers-Brillouin (CWKB) model [38,39] can predict the production cross sections in MNT reactions very well. On the other hand, microscopic models such as the time-dependent Hartree-Fock (TDHF) model [40–42] and the improved quantum molecular dynamics (ImQMD) model [43,44] have achieved reasonable success in describing the dissipative dynamics in deep inelastic collisions.

In this work, we present our study of neutron-rich Pt isotope production through the MNT process using the DNS model. The article is organized as follows. In Sec. II, we describe the DNS model. The results and discussion are presented in Sec. III. Finally, we summarize the main results in Sec. IV.

## II. THE MODEL

In the DNS model, the production cross sections of the primary products with proton number $Z_1$ and neutron number

*Corresponding author: fszhang@bnu.edu.cn

 

TABLE I. A brief summary of the neutron-rich Pt isotopes.

| Reaction | $E_{\rm lab}$ | Method | Isotope | Ref. |
|---|---|---|---|---|
| $^{196}$Pt($^{2}$H, $^{1}$H)$^{197}$Pt | 5 MeV | LP | $^{197}$Pt | [7] |
| $^{198}$Pt$(n,\gamma)^{199}$Pt | 0–1 keV | NC | $^{199}$Pt | [8] |
| $^{199}$Pt$(n,\gamma)^{200}$Pt | – | NC | $^{200}$Pt | [9] |
| $^{204}$Hg$(n,\alpha)^{201}$Pt | 1 MeV | LP | $^{201}$Pt | [10] |
| $^{204}$Hg$(n,2pn)^{202}$Pt | 21 MeV | LP | $^{202}$Pt | [11] |
| $^{208}$Pb + $^{9}$Be | 1 GeV/nucleon | PF | $^{203–204}$Pt | [12] |
| $^{238}$U + $^{9}$Be | 1 GeV/nucleon | PF | $^{205}$Pt | [4] |
| $^{238}$U + $^{9}$Be | 1 GeV/nucleon | PF | $^{206–208}$Pt | [6] |

$N_1$ in transfer processes are calculated by the following expression [45]:

$$\sigma_{\rm pr}(Z_1, N_1, E_{\rm c.m.}) = \frac{\pi\hbar^2}{2\mu E_{\rm c.m.}} \sum_J (2J+1) \times P(Z_1, N_1, t = \tau_{\rm int}(J)). \quad (1)$$

Here, $\mu$ is the reduced mass of the system and $E_{\rm c.m.}$ is the incident energy in the center-of-mass frame. $P$ is the fragment distribution probability. $\tau_{\rm int}$ is the interaction time, which depends on the angular momentum $J$. Subsequent deexcitation processes of the excited fragments are treated with the GEMINI code [46].

The interaction time $\tau_{\rm int}(J)$ is determined by

$$\tau_{\rm int}(J) = \frac{\Delta\theta\,\zeta_{\rm tot}}{J} + \frac{1}{\kappa}\ln\frac{J_{\rm f}}{J}, \quad (2)$$

where $\Delta\theta$ is the rotational angle of the DNS, $\zeta_{\rm tot}$ is the total moment of inertia, $\kappa$ is the fitting parameter, and $J_{\rm f}$ is the final angular momentum. The detailed description of the interaction time can be found in Refs. [47,48].

The distribution probability $P(Z_1, N_1, t)$ for fragment 1 with proton number $Z_1$ and neutron number $N_1$ at time $t$ is obtained by solving the master equation [49,50]

$$\begin{aligned}\frac{dP(Z_1,N_1,t)}{dt} &= \sum_{Z_1'} W_{Z_1,N_1;Z_1',N_1}(t)[d_{Z_1,N_1}P(Z_1',N_1,t) - d_{Z_1',N_1}P(Z_1,N_1,t)] \\ &+ \sum_{N_1'} W_{Z_1,N_1;Z_1,N_1'}(t)[d_{Z_1,N_1}P(Z_1,N_1',t) - d_{Z_1,N_1'}P(Z_1,N_1,t)] \\ &- [\Lambda_{\rm qf}(\Theta(t)) + \Lambda_{\rm fis}(\Theta(t))]P(Z_1,N_1,t). \end{aligned} \quad (3)$$

Here, $W_{Z_1,N_1;Z_1',N_1}$ ($W_{Z_1,N_1;Z_1,N_1'}$) is the mean transition probability from channel $(Z_1, N_1)$ to $(Z_1', N_1)$ [or from $(Z_1, N_1)$ to $(Z_1, N_1')$]. $d_{Z_1,N_1}$ is the microscopic dimension corresponding to the macroscopic state $(Z_1, N_1)$. Only one nucleon transfer process is considered in the DNS model. The sum is taken over all possible proton numbers and neutron numbers that the fragment $(Z_1', N_1')$ may have. $\Lambda_{\rm qf}$ and $\Lambda_{\rm fis}$ describe the quasifission and fission rate in the DNS, respectively, which are calculated by the one-dimensional Kramers equation [50]. The quasifission rate $\Lambda_{\rm qf}$ is determined by the following expression:

$$\Lambda_{\rm qf}(\Theta(t)) = \frac{\omega}{2\pi\omega^{B_{\rm qf}}}\left[\sqrt{\left(\frac{\Gamma}{2\hbar}\right)^2 + (\omega^{B_{\rm qf}})^2} - \frac{\Gamma}{2\hbar}\right] \times \exp\left[-\frac{B_{\rm qf}(Z_1,N_1)}{\Theta(t)}\right]. \quad (4)$$

Here, $\Theta(t)$ is the local temperature determined by the Fermi-gas expression $\Theta = \sqrt{\varepsilon^*/a}$, with the local excitation energy $\varepsilon^*$ and the level-density parameter $a = A/12$ MeV$^{-1}$. The frequency $\omega$ of the harmonic oscillator approximates the interaction potential at the bottom of the pocket, and $\omega^{B_{\rm qf}}$ is the frequency of the harmonic oscillator approximating the potential at the top of the Coulomb barrier. $\Gamma$ denotes the double average width of the single-particle states. In this work, $\Gamma = 2.8$ MeV, $\hbar\omega^{B_{\rm qf}} = 2.0$ MeV, and $\hbar\omega = 3.0$ MeV are used. $B_{\rm qf}(Z_1, N_1)$ is the quasifission barrier corresponding to the fragment $(Z_1, N_1)$.

The fission rate $\Lambda_{\rm fis}$ is calculated by the formula

$$\Lambda_{\rm fis}(\Theta(t)) = \frac{\omega_{\rm g.s.}}{2\pi\omega_{\rm f}}\left[\sqrt{\left(\frac{\Gamma_0}{2\hbar}\right) + (\omega_{\rm f})^2} - \frac{\Gamma_0}{2\hbar}\right] \times \exp\left[-\frac{B_{\rm f}(Z_1,N_1)}{\Theta(t)}\right], \quad (5)$$

where $\omega_{\rm g.s.}$ and $\omega_{\rm f}$ are the frequencies of the oscillators approximating the fission-path potential at the ground state and on the top of the fission barrier, respectively. In our calculations, $\hbar\omega_{\rm g.s.} = \hbar\omega_{\rm f} = 1$ MeV and $\Gamma_0 = 2$ MeV are used. $B_{\rm f}(Z_1, N_1)$ is the fission barrier of the fragment $(Z_1, N_1)$, which is taken to be the sum of a liquid drop part and the shell correction.

The local excitation energy of the DNS is determined by

$$\varepsilon^* = E_{\rm diss} - [U(Z_1,N_1,Z_2,N_2) - U(Z_{\rm p},N_{\rm p},Z_{\rm t},N_{\rm t})] - \frac{(J-M)^2}{2\zeta_{\rm rel}} - \frac{M^2}{2\zeta_{\rm int}}. \quad (6)$$

Here, $E_{\rm diss}$ is the energy dissipating to the DNS system from the relative kinetic energy. $U(Z_1, N_1, Z_2, N_2)$ is the driving potential of the fragment $(Z_1, N_1)$ with $(Z_2, N_2)$, and $U(Z_{\rm p}, N_{\rm p}, Z_{\rm t}, N_{\rm t})$ is the driving potential corresponding to the entrance channel. $\zeta_{\rm rel}$ and $\zeta_{\rm int}$ are relative and intrinsic moments of inertia of the DNS, respectively. $\zeta_{\rm rel}$ is obtained by $\zeta_{\rm rel} = \mu R^2$. $R$ is the position where nucleon transfer takes place and is taken as $R = R_1(1 + \beta_1 Y_{20}(\theta_1)) + R_2(1 + \beta_2 Y_{20}(\theta_2)) + 0.7$ fm. Here, $R_{1,2} = 1.16A_{1,2}^{1/3}$. $\beta_1$ and $\beta_2$ are the quadrupole deformation parameters of the two fragments, which are taken from Ref. [51]. $\theta_{1,2} = 0$ for tip-tip collision. $\zeta_{\rm int}$ is determined by $\zeta_{\rm int} = \zeta_1 + \zeta_2$, where $\zeta_1$ and $\zeta_2$ are the intrinsic angular momenta of fragments 1 and 2, respectively, which are from Ref. [52]. $M$ describes the intrinsic angular momentum from the dissipation of the relative angular momentum, which is obtained from the equation $M = J\,\zeta_{\rm int}/(\zeta_{\rm int} + \zeta_{\rm rel})[1 - \exp(-t/\tau_J)]$. Here, $\tau_J$ is the angular momentum relaxation time.

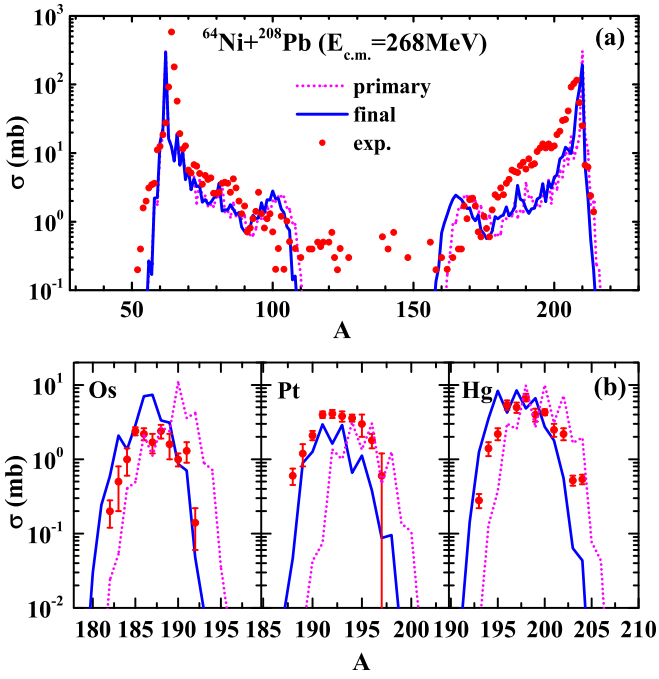


FIG. 1. (a) Mass distributions in $^{64}$Ni + $^{208}$Pb at $E_{\text{c.m.}} =$ 268 MeV. (b) The isotopic production cross sections of Os, Pt, and Hg. The dotted and solid lines denote the calculation results for primary and final fragments, respectively. The experimental data are from Ref. [54].

The diffusion process is driven by the potential energy surface (PES) [31,32] and is defined as

$$\begin{aligned} U(Z_1, N_1, Z_2, N_2, R, \beta_1, \beta_2) \\ = B(Z_1, N_1) + B(Z_2, N_2) \\ + V_{\text{CN}}(Z_1, N_1, Z_2, N_2, R, \beta_1, \beta_2), \end{aligned} \tag{7}$$

where $B(Z_1, N_1)$ and $B(Z_2, N_2)$ are the binding energies of the fragments $(Z_1, N_1)$ and $(Z_2, N_2)$, respectively.

$V_{\text{CN}}$ is the interaction potential of the two fragments, shown as

$$\begin{aligned} V_{\text{CN}}(Z_1, N_1, Z_2, N_2, R, \beta_1, \beta_2) \\ = V_{\text{C}}(Z_1, N_1, Z_2, N_2, R, \beta_1, \beta_2) \\ + V_{\text{N}}(Z_1, N_1, Z_2, N_2, R, \beta_1, \beta_2). \end{aligned} \tag{8}$$

Here, $V_{\text{C}}$ and $V_{\text{N}}$ are the Coulomb potential [53] and nuclear potential [33], respectively.

We first test the DNS model for describing the mass distributions of the MNT reaction in $^{64}$Ni + $^{208}$Pb at $E_{\text{c.m.}} =$ 268 MeV.

As shown in Fig. 1(a), the trend of the system evolution towards symmetric mass distribution can be clearly seen in the mass transfer from target to projectile. We can see that this characteristic is described very well by the DNS model. In addition, we note that the experimental peak value on the target is significantly lower than that on the projectile. This is because that the target-like fragments (TLFs) have larger excitation energy during the collisions. In the deexcitation process, the TLFs emit more neutrons than the projectile-like fragments (PLFs).

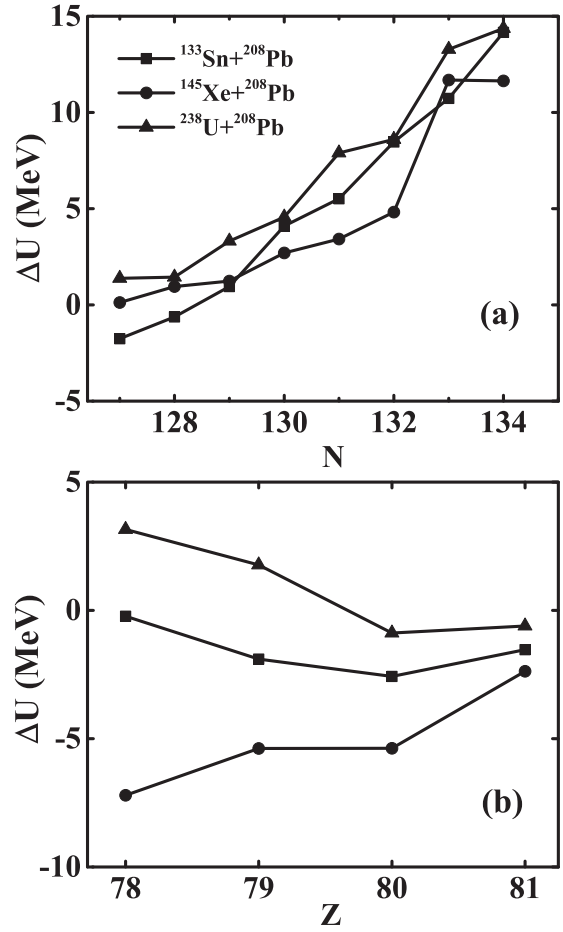


FIG. 2. $\Delta U$ values in the pure neutron pickup (a) and pure proton stripping (b) channels in the transfer reactions $^{145}$Xe + $^{208}$Pb, $^{133}$Sn + $^{208}$Pb, and $^{238}$U + $^{208}$Pb.

This phenomenon is also found in the DNS calculations (solid line). Figure 1(b) shows the isotopic production cross sections of Os, Pt, and Hg. One can see that final yields shift to the left after the deexcitation process. The final isotopic cross sections are in good agreement with the experimental data. These results indicate that the DNS model is applicable for the study of MNT reactions at near barrier energies.

## III. RESULTS AND DISCUSSION

Considering that the production cross sections at the maximum of the isotopic distributions decrease rapidly with increasing proton transfer channel, we choose nuclei in the vicinity of Pt as targets to study the production of the extremely neutron-rich nuclei of Pt. The value of the driving potential needed to overcome $(\Delta U)$ is crucial to drive the nuclear reactions. A smaller $\Delta U$ value generally results in a relatively high production cross section for the primary products.

Figure 2 shows the $\Delta U$ value along the pure neutron pickup (a) and pure proton stripping (b) channels in the transfer reactions $^{133}$Sn + $^{208}$Pb, $^{145}$Xe + $^{208}$Pb, and $^{238}$U + $^{208}$Pb. Stripping channels correspond to nucleon transfer from the target to the projectile, while pickup channels correspond to

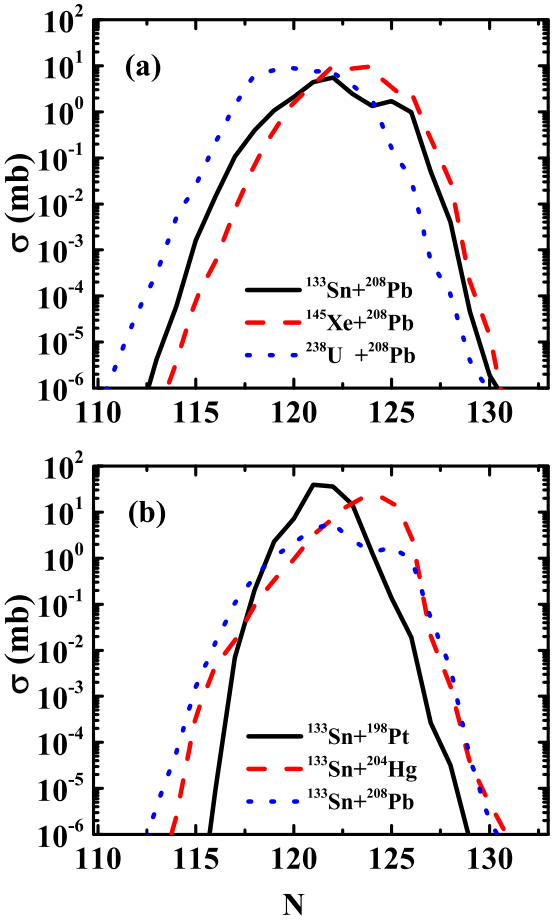


FIG. 3. (a) Final isotopic production cross sections of Pt with $^{133}$Sn + $^{208}$Pb, $^{145}$Xe + $^{208}$Pb, and $^{238}$U + $^{208}$Pb reactions at $E_{\text{c.m.}} = 1.10V_{\text{C}}$. (b) Final isotopic production cross sections of Pt with $^{133}$Sn + $^{198}$Pt, $^{133}$Sn + $^{204}$Hg, and $^{133}$Sn + $^{208}$Pb reactions at $E_{\text{c.m.}} = 1.10V_{\text{C}}$.

the opposite. From the Fig. 2(a), one can see that the $\Delta U$ value increases with increasing number of neutron pickup, and the value for $^{145}$Xe + $^{208}$Pb system is almost the smallest in the larger neutron pickup channel. This means that the neutron pickup in the $^{145}$Xe + $^{208}$Pb reaction is easier than that in $^{133}$Sn + $^{208}$Pb and $^{238}$U + $^{208}$Pb reactions.

On the other hand, for the pure proton stripping channel [Fig. 2(b)], the increase of proton transfer leads to more and more difference of $\Delta U$ for these three systems. The $\Delta U$ value becomes larger with increasing number of proton stripping in the $^{133}$Sn + $^{208}$Pb and $^{238}$U + $^{208}$Pb reactions, but the $^{145}$Xe + $^{208}$Pb reaction shows an opposite trend. This indicates that the proton stripping for $^{145}$Xe + $^{208}$Pb is easier compared to the $^{133}$Sn + $^{208}$Pb and $^{238}$U + $^{208}$Pb reactions. In order to produce new neutron-rich Pt isotopes, it is expected that the target loses protons and obtains neutrons during the reactions. Hence, $^{145}$Xe + $^{208}$Pb should be a favorable candidate.

Figure 3(a) presents the final isotopic production cross sections of Pt in $^{133}$Sn + $^{208}$Pb, $^{145}$Xe + $^{208}$Pb, and $^{238}$U + $^{208}$Pb reactions at $E_{\text{c.m.}} = 1.10V_{\text{C}}$. These reactions have the same target, $^{208}$Pb, only the projectiles are different. One can see that the production cross sections on the neutron-rich side for the $^{145}$Xe + $^{208}$Pb reaction are largest. This is due to smallest $\Delta U$ values along the neutron pickup and proton stripping channels, as shown in the Figs. 2(a) and 2(b), respectively. In fact, the $\Delta U$ values are influenced by the nuclear symmetry energy. The production of neutron-rich nuclei is closely related to the $N/Z$ ratio equilibration process between the projectile and target during the collisions. The $N/Z$ ratio of $^{238}$U is 1.587, which is smaller compared to $^{133}$Sn (1.685) and $^{145}$Xe (1.660). The $N/Z$ ratio of $^{208}$Pb is 1.538. Hence, the isotopic production cross sections of Pt from the $^{238}$U + $^{208}$Pb reaction on the neutron-rich side are lowest.

Figure 3(b) shows the final isotopic production cross sections of Pt in the reactions of $^{133}$Sn with $^{198}$Pt, $^{204}$Hg, and $^{208}$Pb targets at $E_{\text{c.m.}} = 1.10V_{\text{C}}$. The $N/Z$ ratios of $^{198}$Pt, $^{204}$Hg, and $^{208}$Pb are almost the same, i.e., 1.537, 1.55 and 1.538, respectively. However the proton stripping channels from the target to Pt are $0p$, $-2p$, and $-4p$, respectively. One can see that the $^{133}$Sn + $^{198}$Pt reaction is nonideal for producing the extremely neutron-rich nuclei of Pt. This is because the larger pure neutron pickup is very difficult in the reaction. In the $N/Z$ ratio equilibration processes, the neutron pickup channel is usually accompanied with a proton stripping channel. The $^{133}$Sn + $^{204}$Hg and $^{133}$Sn + $^{208}$Pb reactions have larger advantage for producing the neutron-rich nuclei of Pt, because $^{204}$Hg just needs the stripping of two protons to reach Pt. Although $^{208}$Pb needs to lose four protons to reach the Pt, it requires a smaller number of neutron pickup to generate the extremely neutron-rich Pt than $^{204}$Hg.

The final isotopic production cross sections of Pt for the reactions $^{145}$Xe + $^{208}$Pb and $^{133}$Sn + $^{204}$Hg at different incident energies are shown in Fig. 4. The solid circles denote the experimental data of 1 GeV/$A$ $^{238}$U + $^{9}$Be performed at GSI [6]. The blank circle, square, and triangle symbols denote the unknown neutron-rich isotopes produced at $E_{\text{c.m.}} = 1.10V_{\text{C}}$, $1.14V_{\text{C}}$, $1.18V_{\text{C}}$, respectively. From Figs. 4(a) and 4(b) one can see that, on the neutron-rich side, the production cross sections are not sensitive to the incident energy compared to the neutron-deficient side, because larger incident energy improves the transfer probability of nucleons. However, larger incident energy will result in a higher excitation energy for primary fragments. More neutrons evaporating causes a shift of final yields to the neutron-deficient side. In addition, we find that the production cross sections of Pt on the neutron-rich side are extremely higher than those produced in the PF method. There are serval new neutron-rich isotopes, $^{209–212}$Pt, that could be produced by these two systems.

In order to find the optimal incident energy, the production cross sections of $^{209–212}$Pt in the reaction $^{133}$Sn + $^{204}$Hg and $^{145}$Xe + $^{208}$Pb at $E_{\text{c.m.}} = 1.10V_{\text{C}}$, $1.14V_{\text{C}}$, $1.18V_{\text{C}}$, $1.30V_{\text{C}}$, $1.40V_{\text{C}}$, and $1.50V_{\text{C}}$ are shown in Table II. It is obvious that the yield becomes lower with more neutrons transferred at the same incident energy for these two reactions due to larger and larger $\Delta U$ value. The largest production cross sections of $^{209–212}$Pt in the reaction $^{133}$Sn + $^{204}$Hg locate at $E_{\text{c.m.}} = 1.18\ V_{\text{C}}$, in which the values are 1.7 nb, 0.4 nb, 23.3 pb, and 4.8 pb, respectively. However, the optimal incident energy for $^{145}$Xe + $^{208}$Pb is larger than that for $^{133}$Sn + $^{204}$Hg. The highest cross sections of $^{209–212}$Pt are 2.7 nb, 0.4 nb, 8.2 pb, and 2.7 pb at $E_{\text{c.m.}} = 1.30V_{\text{C}}$, $1.40V_{\text{C}}$, $1.50V_{\text{C}}$, and $1.40V_{\text{C}}$, respectively.

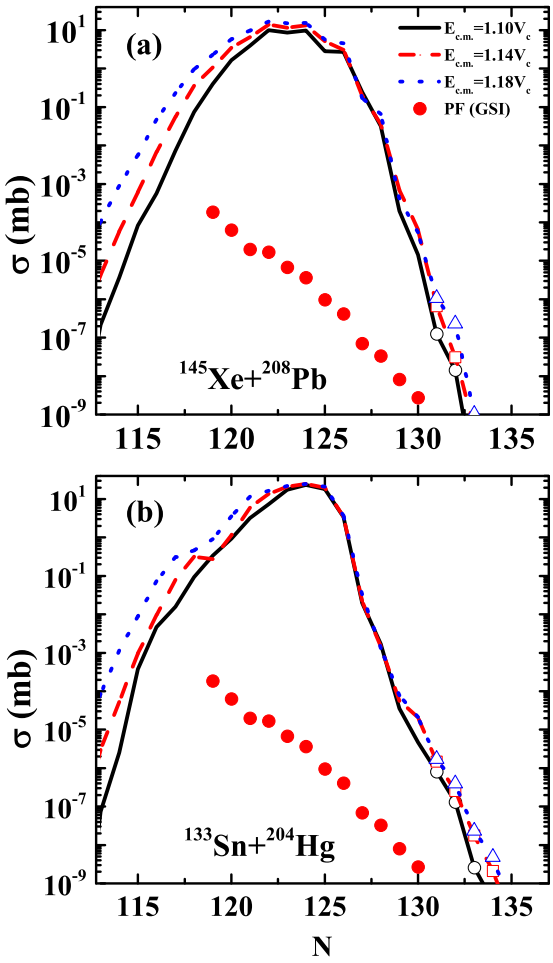


FIG. 4. Final isotopic production cross sections of Pt in $^{145}$Xe + $^{208}$Pb (a) and $^{133}$Sn + $^{204}$Hg (b) at $E_{c.m.} = 1.10V_C$, $1.14V_C$, and $1.18V_C$. The solid circles are experimental data of 1 GeV/$A$ $^{238}$U + $^{9}$Be from Ref. [6]. The blank circle, square, and triangle symbols denote the unknown neutron-rich isotopes produced at $E_{c.m.} = 1.10V_C$, $1.14V_C$, $1.18V_C$, respectively. The production cross sections of the unknown isotopes can be found in Table II.

TABLE II. The production cross sections of $^{209-212}$Pt isotopes. $\Delta U^{Xe+Pb}$ and $\Delta U^{Sn+Hg}$ are the $\Delta U$ values of $^{145}$Xe + $^{208}$Pb and $^{133}$Sn + $^{204}$Hg reactions, respectively. $\sigma^{Xe+Pb}$ and $\sigma^{Sn+Hg}$ are the production cross sections of these two systems, respectively.

| Isotope | $\Delta U^{Xe+Pb}$ | $\Delta U^{Sn+Hg}$ | $E_{c.m.}/V_C$ | $\sigma^{Xe+Pb}$ (pb) | $\sigma^{Sn+Hg}$ (pb) |
|---|---|---|---|---|---|
| $^{209}$Pt | 7.62 MeV | 16.42 MeV | 1.10 | 123.1 | 813.4 |
| | | | 1.14 | 657.1 | 1471 |
| | | | 1.18 | 1066.0 | 1690 |
| | | | 1.30 | 2684.8 | 779.9 |
| | | | 1.40 | 2641.7 | 501.8 |
| | | | 1.50 | 965.8 | 165.1 |
| $^{210}$Pt | 10.73 MeV | 17.37 MeV | 1.10 | 14.2 | 131.4 |
| | | | 1.14 | 31.1 | 254.7 |
| | | | 1.18 | 227.6 | 389.5 |
| | | | 1.30 | 113.3 | 176.5 |
| | | | 1.40 | 418.2 | 97.2 |
| | | | 1.50 | 52.0 | 77.9 |
| $^{211}$Pt | 21.20 MeV | 20.14 MeV | 1.10 | | 2.6 |
| | | | 1.14 | | 17.7 |
| | | | 1.18 | 1.0 | 23.3 |
| | | | 1.30 | 5.1 | 14.3 |
| | | | 1.40 | 7.6 | 7.7 |
| | | | 1.50 | 8.2 | 4.9 |
| $^{212}$Pt | 21.47 MeV | 23.85 MeV | 1.10 | | |
| | | | 1.14 | | 2.1 |
| | | | 1.18 | | 4.8 |
| | | | 1.30 | 2.2 | 3.4 |
| | | | 1.40 | 2.7 | 2.1 |
| | | | 1.50 | 1.9 | |

It is recognized that the beam intensity plays an important role in the experiment to produce unknown isotopes. The factor "cross section × beam intensity" ($\sigma \times \phi$) can be a criterion to judge if the projectile-target combination is suitable. Figure 5 shows the values of $\sigma \times \phi$ for the $^{145}$Xe + $^{208}$Pb and $^{133}$Sn + $^{204}$Hg reactions for producing the nuclei $^{209-212}$Pt at the optimal incident energy. The estimated beam intensities proposed in the SPIRAL2 project for $^{133}$Sn and $^{145}$Xe are taken from Ref. [55]. It is found that the advantage of $^{145}$Xe + $^{208}$Pb reaction gets more apparent for producing the neutron-rich nuclei of Pt, mainly due to the more obvious advantage of production cross section and beam intensity.

## IV. CONCLUSIONS

In conclusion, the multinucleon transfer reaction $^{64}$Ni + $^{208}$Pb at $E_{c.m.} = 268$ MeV is investigated by the DNS model. The results show that the mass distributions and the isotopic distributions agree with the experimental data very well. The $\Delta U$ value increases with increasing the number of neutron pickup and the value for thee $^{145}$Xe + $^{208}$Pb system is almost the smallest in the larger neutron pickup channel. For the pure proton stripping channel, the $\Delta U$ value becomes larger with

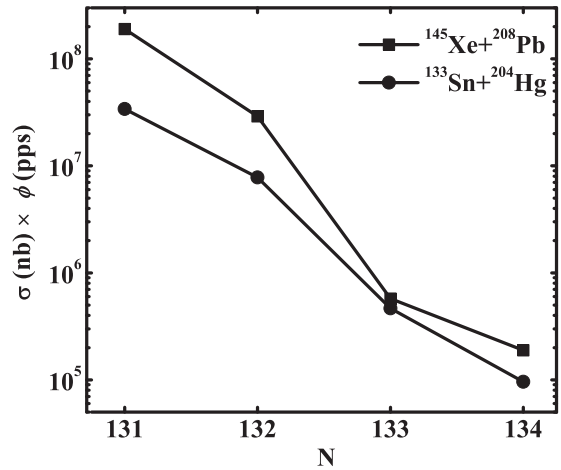


FIG. 5. "Cross section × beam intensity" factor ($\sigma \times \phi$) in collisions of $^{133}$Sn + $^{204}$Hg and $^{145}$Xe + $^{208}$Pt for production of nuclei $^{209-212}$Pt at the optimal incident energy. The estimated beam intensities are proposed in SPIRAL2 [55].

increasing number of proton stripping in the $^{133}$Sn + $^{208}$Pb and $^{238}$U + $^{208}$Pb reactions, but the $^{145}$Xe + $^{208}$Pb reaction shows an opposite trend. This indicates that $^{145}$Xe + $^{208}$Pb system is a good combination to produce extremely neutron-rich nuclei of Pt. The optimal incident energy to obtain $^{209–212}$Pt isotopes in the reaction $^{133}$Sn + $^{204}$Hg is $1.18V_C$. The corresponding production cross sections are 2.7 nb, 0.4 nb, 8.2 pb, and 2.7 pb, respectively. The optimal incident energy for the $^{145}$Xe + $^{208}$Pb system is about $1.40V_C$, and the highest cross sections of unknown isotopes $^{209–212}$Pt are 1.7 nb, 0.4 nb, 23.3 pb, and 4.8 pb, respectively. By analyzing the beam intensity factor, we find that the $^{145}$Xe + $^{208}$Pb system is advantageous to produce $^{209–212}$Pt.

## ACKNOWLEDGMENTS

This work was supported by the National Natural Science Foundation of China under Grants No. 11635003, No. 11025524, and No. 11161130520; the National Basic Research Program of China under Grant No. 2010CB832903; and the European Commissions 7th Framework Programme (Fp7-PEOPLE-2010-IRSES) under Grant No. 269131.

[1] E. M. Burbidge, G. R. Burbidge, W. A. Fowler, and F. Hoyle, Rev. Mod. Phys. **29**, 547 (1957).
[2] M. Arnould, S. Goriely, and K. Takahashi, Phys. Rep. **450**, 97 (2007).
[3] M. Pfützner, P. Armbruster, T. Baumann, J. Benlliure, M. Bernas, W. N. Catford, D. Cortina-Gil, J. M. Daugas, H. Geissel, M. Górska, H. Grawe, R. Grzywacz, M. Hellström, N. Iwasa, Z. Janas, A. R. Junghans, M. Karny, S. Leenhardt, M. Lewitowicz, A. C. Mueller, F. de Oliviera, P. H. Regan, M. Rejmund, K. Rykaczewski, and K. Sümmerer, Phys. Lett. B **444**, 32 (1998).
[4] H. Alvarez-Pol, J. Benlliure, E. Casarejos, L. Audouin, D. Cortina-Gil, T. Enqvist, B. Fernández-Domínguez, A. R. Junghans, B. Jurado, P. Napolitani, J. Pereira, F. Rejmund, K. H. Schmidt, and O. Yordanov, Phys. Rev. C **82**, 041602 (2010).
[5] A. I. Morales, J. Benlliure, J. Agramunt, A. Algora, N. Alkhomashi, H. Álvarez-Pol, P. Boutachkov, A. M. Bruce, L. S. Cáceres, E. Casarejos, A. M. DenisBacelar, P. Doornenbal, D. Dragosavac, G. Farrelly, A. Gadea, W. Gelletly, J. Gerl, M. Górska, J. Grebosz, I. Kojouharov, F. Molina, D. Pérez-Loureiro, S. Pietri, Z. Podolyák, P. H. Regan, B. Rubio, H. Shaffner, S. J. Steer, S. Tashenov, S. Verma, and H. J. Wollersheim, Phys. Rev. C **84**, 011601 (2011).
[6] J. Kurcewicz, F. Farinon, H. Geissel, S. Pietri, C. Nociforo, A. Prochazka, H. Weick, J. S. Winfield, A. Estradé, P. R. P. Allegro, A. Bail, G. Bélier, J. Benlliure, G. Benzoni, M. Bunce, M. Bowry, R. Caballero-Folch, I. Dillmann, A. Evdokimov, J. Gerl, A. Gottardo, E. Gregor, R. Janik, A. Kelić-Heil, R. Knöbel, T. Kubo, Y. A. Litvinov, E. Merchan, I. Mukha, F. Naqvi, M. Pfützner, M. Pomorski, Z. Podolyák, P. H. Regan, B. Riese, M. V. Ricciardi, C. Scheidenberger, B. Sitar, P. Spiller, J. Stadlmann, P. Strmen, B. Sun, I. Szarka, J. Taïeb, S. Terashima, J. J. Valiente-Dobón, M. Winkler, and P. Woods, Phys. Lett. B **717**, 371 (2012).
[7] J. M. Cork and E. O. Lawrence, Phys. Rev. **49**, 788 (1936).
[8] E. McMillan, M. Kamen, and S. Ruben, Phys. Rev. **52**, 375 (1937).
[9] L. P. Roy, J. C. Roy, and J. S. Merritt, Phys. Rev. **105**, 1337 (1957).
[10] J. Facetti, E. Trabal, R. McClin, and S. Torres, Phys. Rev. **127**, 1690 (1962).
[11] S. Shi, W. D. Huang, Y. Li, D. Z. Yin, J. H. Gu, and J. Q. Tian, Z. Phys. A **342**, 369 (1992).
[12] S. J. Steer, Z. Podolyák, S. Pietri, M. Górska, P. H. Regan, D. Rudolph, E. Werner-Malento, A. B. Garnsworthy, R. Hoischen, J. Gerl, H. J. Wollersheim, K. H. Maier, H. Grawe, F. Becker, P. Bednarczyk, L. Cáceres, P. Doornenbal, H. Geissel, J. Grebosz, A. Kelic, I. Kojouharov, N. Kurz, F. Montes, W. Prokopowicz, T. Saito, H. Schaffner, S. Tashenov, A. Heinz, M. Pfützner, T. Kurtukian-Nieto, G. Benzoni, A. Jungclaus, D. L. Balabanski, C. Brandau, B. A. Brown, A. M. Bruce, W. N. Catford, I. J. Cullen, Z. Dombrádi, M. E. Estevez, W. Gelletly, G. Ilie, J. Jolie, G. A. Jones, M. Kmiecik, F. G. Kondev, R. Krücken, S. Lalkovski, Z. Liu, A. Maj, S. Myalski, S. Schwertel, T. Shizuma, P. M. Walker, and O. Wieland, Phys. Rev. C **78**, 061302 (2008).
[13] G. G. Adamian, N. V. Antonenko, and A. S. Zubov, Phys. Rev. C **71**, 034603 (2005).
[14] V. Zagrebaev and W. Greiner, Phys. Rev. Lett. **101**, 122701 (2008).
[15] V. Zagrebaev and W. Greiner, J. Phys. G: Nucl. Part. Phys. **35**, 125103 (2008).
[16] G. G. Adamian, N. V. Antonenko, V. V. Sargsyan, and W. Scheid, Phys. Rev. C **81**, 057602 (2010).
[17] M. H. Mun, G. G. Adamian, N. V. Antonenko, Y. Oh, and Y. Kim, Phys. Rev. C **89**, 034622 (2014).
[18] M. H. Mun, G. G. Adamian, N. V. Antonenko, Y. Oh, and Y. Kim, Phys. Rev. C **91**, 054610 (2015).
[19] M. H. Mun, G. G. Adamian, N. V. Antonenko, and Y. O. Lee, Eur. Phys. J. A **52**, 363 (2016).
[20] V. F. Comas, S. Heinz, S. Hofmann, D. Ackermann, J. A. Heredia, F. P. Heßberger, J. Khuyagbaatar, B. Kindler, B. Lommel, and R. Mann, Eur. Phys. J. A **49**, 112 (2013).
[21] O. Beliuskina, S. Heinz, V. Zagrebaev, V. Comas, C. Heinz, S. Hofmann, R. Knöbel, M. Stahl, D. Ackermann, F. P. Heßberger, B. Kindler, B. Lommel, J. Maurer, and R. Mann, Eur. Phys. J. A **50**, 161 (2014).
[22] Y. X. Watanabe, Y. H. Kim, S. C. Jeong, Y. Hirayama, N. Imai, H. Ishiyama, H. S. Jung, H. Miyatake, S. Choi, J. S. Song, E. Clement, G. de France, A. Navin, M. Rejmund, C. Schmitt, G. Pollarolo, L. Corradi, E. Fioretto, D. Montanari, M. Niikura, D. Suzuki, H. Nishibata, and J. Takatsu, Phys. Rev. Lett. **115**, 172503 (2015).
[23] J. S. Barrett, W. Loveland, R. Yanez, S. Zhu, A. D. Ayangeakaa, M. P. Carpenter, J. P. Greene, R. V. F. Janssens, T. Lauritsen, E. A. McCutchan, A. A. Sonzogni, C. J. Chiara, J. L. Harker, and W. B. Walters, Phys. Rev. C **91**, 064615 (2015).
[24] E. M. Kozulin, E. Vardaci, G. N. Knyazheva, A. A. Bogachev, S. N. Dmitriev, I. M. Itkis, M. G. Itkis, A. G. Knyazev, T. A. Loktev, K. V. Novikov, E. A. Razinkov, O. V. Rudakov, S. V. Smirnov, W. Trzaska, and V. I. Zagrebaev, Phys. Rev. C **86**, 044611 (2012).

[25] T. Welsh, W. Loveland, R. Yanez, J. S. Barrett, E. A. McCutchan, A. A. Sonzogni, T. Johnson, S. Zhu, J. P. Greene, A. D. Ayangeakaa, M. P. Carpenter, T. Lauritsen, J. L. Harker, W. B. Walters, B. M. S. Amro, and P. Copp, Phys. Lett. B **771**, 119 (2017).
[26] E. M. Kozulin, V. I. Zagrebaev, G. N. Knyazheva, I. M. Itkis, K. V. Novikov, M. G. Itkis, S. N. Dmitriev, I. M. Harca, A. E. Bondarchenko, A. V. Karpov, V. V. Saiko, and E. Vardaci, Phys. Rev. C **96**, 064621 (2017).
[27] V. I. Zagrebaev and W. Greiner, Phys. Rev. C **83**, 044618 (2011).
[28] A. V. Karpov and V. V. Saiko, Phys. Rev. C **96**, 024618 (2017).
[29] Z. Q. Feng, Phys. Rev. C **95**, 024615 (2017).
[30] L. Zhu, J. Su, W. J. Xie, and F. S. Zhang, Phys. Lett. B **767**, 437 (2017).
[31] G. G. Adamian, N. V. Antonenko, and W. Scheid, Nucl. Phys. A **618**, 176 (1997).
[32] G. G. Adamian, N. V. Antonenko, W. Scheid, and V. V. Volkov, Nucl. Phys. A **633**, 409 (1998).
[33] Z. Q. Feng, G. M. Jin, J. Q. Li, and W. Scheid, Phys. Rev. C **76**, 044606 (2007).
[34] A. Winther, Nucl. Phys. A **594**, 203 (1995).
[35] L. Corradi, G. Pollarolo, and S. Szilner, J. Phys. G: Nucl. Part. Phys. **36**, 113101 (2009).
[36] V. Zagrebaev and W. Greiner, J. Phys. G: Nucl. Part. Phys. **34**, 2265 (2007).
[37] V. I. Zagrebaev, B. Fornal, S. Leoni, and W. Greiner, Phys. Rev. C **89**, 054608 (2014).
[38] E. Vigezzi and A. Winther, Ann. Phys. (NY) **192**, 432 (1989).
[39] S. Szilner, L. Corradi, G. Pollarolo, S. Beghini, R. B. Behera, E. Fioretto, A. Gadea, F. Haas, A. Latina, G. Montagnoli, F. Scarlassara, A. M. Stefanini, M. Trotta, A. M. Vinodkumar, and Y. Wu, Phys. Rev. C **71**, 044610 (2005).
[40] J. W. Negele, Rev. Mod. Phys. **54**, 913 (1982).
[41] K. T. R. Davies and S. E. Koonin, Phys. Rev. C **23**, 2042 (1981).
[42] K. Sekizawa, Phys. Rev. C **96**, 014615 (2017).
[43] N. Wang, K. Zhao, and Z. X. Li, Phys. Rev. C **90**, 054610 (2014).
[44] C. Li, F. Zhang, J. Li, L. Zhu, J. Tian, N. Wang, and F. S. Zhang, Phys. Rev. C **93**, 014618 (2016).
[45] L. Zhu, F. S. Zhang, P. W. Wen, J. Su, and W. J. Xie, Phys. Rev. C **96**, 024606 (2017).
[46] R. J. Charity, M. A. McMahan, G. J. Wozniak, R. J. McDonald, and L. G. Moretto, Nucl. Phys. A **483**, 371 (1988).
[47] G. Wolschin and W. Nörenberg, Z. Phys. A **284**, 209 (1978).
[48] J. Q. Li and G. Wolschin, Phys. Rev. C **27**, 590 (1983).
[49] S. Ayik, B. Schürmann, and W. Nörenberg, Z. Phys. A **277**, 299 (1976).
[50] G. G. Adamian, N. V. Antonenko, and W. Scheid, Phys. Rev. C **68**, 034601 (2003).
[51] P. Möller, J. R. Nix, W. D. Myers, and W. J. Swiatecki, At. Data Nucl. Data Tables **59**, 185 (1995).
[52] A. Naasirov, A. Fukushima, Y. Toyoshima, Y. Aritomo, A. Muminov, S. Kalandarov, and R. Utamuratov, Nucl. Phys. A **759**, 342 (2005).
[53] C. Y. Wong, Phys. Rev. Lett. **31**, 766 (1973).
[54] W. Królas, R. Broda, B. Fornal, T. Pawłat, H. Grawe, K. H. Maier, M. Schramm, and R. Schubart, Nucl. Phys. A **724**, 289 (2003).
[55] S. Gales, Prog. Part. Nucl. Phys. **59**, 22 (2007).